Chemical Physics 76 (1983) 195–202
North-Holland Publishing Company

CALCULATED RO-VIBRATIONAL FINE-STRUCTURE SPECTRUM AND WEAK-FIELD ZEEMAN SPLITTINGS OF THE O_2Ar VAN DER WAALS MOLECULE

Jonathan TENNYSON ‡

Instituut voor Theoretische Chemie, Katholieke Universiteit, Toernooiveld, 6525 ED Nijmegen, The Netherlands

and

Jacques METTES

Fysisch Laboratorium, Katholieke Universiteit, Toernooiveld, 6525 ED Nijmegen, The Netherlands

Received 18 November 1982

Ro-vibrational calculations are performed on O_2Ar explicitly including coupling to the O_2 electronic spin. Two different empirical potentials are used and give similar fine-structure spectra. The anisotropy in the potential is found to strongly perturb the O_2 fine-structure spectrum suggesting that the O_2Ar fine-structure spectrum can give detailed information about the anisotropy of the van der Waals interaction potential. Transition strengths for the complex fine-structure transitions are calculated and found to vary by two orders of magnitude. The Zeeman splitting of the levels by interaction with a weak magnetic field is also calculated.

1. Introduction

There has been much recent interest, both theoretical and experimental, in van der Waals molecules [1]. The study of the dynamics of these loosely bound complexes has led to the development of special techniques capable of representing large ro-vibrational modes in one or more dimensions [2–7]. Given a potential energy surface for a system, these methods can give accurate predictions of ro-vibrational spectra.

Recently, Reuss and co-workers [8,9] have measured the hyperfine spectrum of H_2–X (X = inert gas, H_2) van der Waals molecules. By use of a vector model [10], they were able to invert these data to obtain accurate information about the van der Waals potential in the bonding region. In particular their data probed the leading anisotropic term, $V_2(R)$, to which other experiments are often less sensitive. The vector model, which treats L, the end-over-end rotation of the complex, as a good quantum number is appropriate to H_2 complexes because of the large splitting (≈ 350 cm^{-1}) between the H_2 rotational states. This allows the coupling between rotational states to be neglected to a very good approximation [5].

Oxygen is an interesting species because of its paramagnetic electronic ground state. Coupling to this $^3\Sigma_g^-$ state leads to the characteristic fine structure of O_2 ro-vibrational states; fine-structure transitions lie largely in the 60 GHz region [11]. These levels are further split in a magnetic field by Zeeman interaction [12]. ^{16}O has zero nuclear spin meaning that there is no nuclear hyperfine interaction; Bose–Einstein statistics forbids even rotational states in the $^3\Sigma_g^-$ ground state.

‡ Present address: SERC Daresbury Laboratory, Daresbury, Warrington, Cheshire, WA4 4AD, UK.

0301-0104/83/0000–0000/$03.00

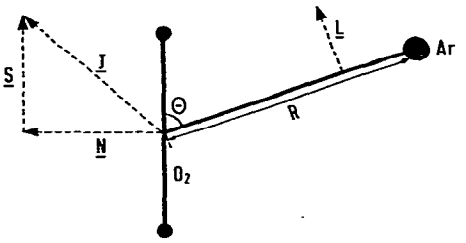

Fig. 1. Coupling scheme used for the O_2Ar calculations $((NS)JL)F$, where the angular momentum vectors are defined in the text.

The ro-vibrational states of van der Waals complexes of O_2 will also be split by spin–orbit interactions. Observation of these splittings could yield valuable information about the van der Waals interaction potential. However, the small splitting between O_2 rotational states (≈ 2.8 cm^{-1}) means that rotational states can be strongly coupled in the dimer, making the use of the vector model inappropriate.

Two empirically motivated interaction potentials for the O_2Ar van der Waals dimer are available [13,14]. Both are expressed as Legendre expansions in $\cos\theta$

$$V(R,\theta)=\sum_{\lambda} V_{\lambda}(R)P_{\lambda}(\cos\theta), \tag{1}$$

truncated at $\lambda = 2$; only λ even contributes by symmetry. R and θ are defined in fig. 1. The Mingelgrin and Gordon $V_{\lambda}(R)$ have an R^{-6}-exponential form [13], whereas those of Pirani and Vecchiocattivi are based on a more sophisticated fit to a variety of experimental data [14].

In this work we use these potentials to calculate the low-temperature fine-structure spectrum for O_2–Ar. We used a method capable of giving all the ro-vibrational states of the complex and a coupling scheme analogous to that of the vector model [10]. This approach uses no approximate quantum numbers. From these levels we obtain Boltzmann distributions for several temperatures. With these distributions and the relevant transition dipole moments one can make predictions of the signal-to-noise ratio of the dimer transitions relative to pure O_2. These ratios are important if the fine structure of the O_2Ar complex is to be observed. Our calculations also allow us to assess what information could be expected from such an experiment and in what region one would expect to see transitions. Finally, we also consider how the low-lying levels of the complex are split by interaction with a weak magnetic field.

2. Method

In the absence of a magnetic field the hamiltonian for the problem can be written as

$$\hat{H}=\hat{H}_{\mathrm{VR}}+\hat{H}_{\mathrm{fine}}. \tag{2}$$

$\hat{H}_{\mathrm{VR}}$ is the usual space-fixed vibration–rotation hamiltonian for the interaction of an atom with a rigid diatom [2]

$$\hat{H}_{\mathrm{VR}}=\frac{-\hbar^2}{2\mu R}\left(\frac{\partial^2}{\partial R^2}\right)R+\frac{\hat{L}^2}{2\mu R^2}+B_{O_2}\hat{N}^2+V(R,\theta), \tag{3}$$

where $\mu = m_a m_d/(m_a + m_d)$, with m_a and m_d being the atomic and diatomic masses respectively; B_{O_2} is the rotational constant of O_2, for which a value of 43.1005 GHz [15] was used. The eigenfunctions of the operators $\hat{L}^2$ and $\hat{N}^2$ are spherical harmonics $|LM_L\rangle$ and $|NM_N\rangle$ with eigenvalues $L(L+1)$ and $N(N+1)$.

$\hat{H}_{\mathrm{fine}}$ consists of the terms which couple the O_2 electronic spin to the orbital motion. For this we have used the same hamiltonian as is appropriate for pure O_2, for which Hund's rule case (b) applies [15].

Following Mizushima [15], $\hat{\boldsymbol{H}}_{\rm fine}$ comprises a spin–orbit coupling term and a Coriolis term

$$\hat{\boldsymbol{H}}_{\rm fine} = \mu_0 \hat{\boldsymbol{N}} \cdot \hat{\boldsymbol{S}} + \tfrac{2}{3}\lambda_0 \left(3\hat{S}_\xi^2 - \hat{\boldsymbol{S}}^2\right), \tag{4}$$

where S_ξ is the projection of $\boldsymbol{S}$ on the O_2 bond axis. For $^{16}O_2$ $\mu_0 = -0.252585$ GHz and $\lambda_0 = 59.501342$ GHz [15]. The operators $\hat{S}_\xi^2$ and $\hat{\boldsymbol{S}}^2$ act on the spin functions $|SM_S\rangle$.

Following Waaijer et al. [10] angular basis functions were taken as coupled spherical harmonics in the form $|((NS)JL)FM_F\rangle$. $|NM_N\rangle$ represents the O_2 rotations, N must be odd, and $|SM_S\rangle$ the angular momentum of the spin, for the ground state $S = 1$. These couple to $|JM_J\rangle$, where J and M_J are the total angular momentum quantum numbers of pure O_2 [15]. In the dimer $|JM_J\rangle$ couples with $|LM_L\rangle$, the end-over-end rotations of the complex, to give $|FM_F\rangle$. F, M_F and the parity $p = (-1)^{N-S+L-1}$ are the only good quantum numbers of the complex. Fig. 1 illustrates this coupling scheme. Previous [1,2] atom–diatom ro-vibrational calculations performed on $S = 0$ systems have used the simplified coupling scheme $|(NL)FM_F\rangle$.

To our angular basis set, we added a set of radial functions generated numerically by explicit integration of the pseudo-diatomic problem obtained by considering $N = 0$, $L = 0$ and $V(R, \theta) = V_0(R)$, see ref. [7] for details. This gives a total basis set which can be written as

$$\{\, \chi_q(R) | ((NS)JL)FM_F\rangle;\, N, q\}. \tag{5}$$

As with previous work [2,5–7], all possible functions with $q \leqslant q_{\max}$ and $N \leqslant N_{\max}$ were included in the basis.

Matrix elements over the radial operators in $\hat{\boldsymbol{H}}_{\rm VR}$ were obtained by explicit numerical integration [2,7]. Matrix elements of the angular functions were obtained by use of the Wigner–Eckart theorem and successive decoupling of the resulting reduced matrix elements [16].

Writing $\langle i| = \langle((NS)JL)FM_F|$ and $|f\rangle = |((N'S)J'L')F'M_F'\rangle$ we obtain

$$\langle i|P_\lambda(\cos\theta)|f\rangle = \delta_{FF'}\delta_{M_F M_F'}(-1)^{F+S+J+J'}\left[(2L+1)(2L'+1)(2N+1)(2N'+1)(2J+1)(2J'+1)\right]^{1/2}$$
$$\times \begin{pmatrix} L & \lambda & L' \\ 0 & 0 & 0 \end{pmatrix} \begin{pmatrix} N & \lambda & N' \\ 0 & 0 & 0 \end{pmatrix} \begin{Bmatrix} J & \lambda & J' \\ L' & F & L \end{Bmatrix} \begin{Bmatrix} N & \lambda & N' \\ J' & S & J \end{Bmatrix}. \tag{6}$$

for the angular integral over the potential expressed in the form (1), where the 3-j and 6-j symbols are standard [17]. Writing $S = 0$ reduces this to the more common Percival–Seaton coefficient [18].

As $\hat{\boldsymbol{H}}_{\rm fine}$ contains only scalar operators, its matrix elements are unaffected by complex formation: they are [15]

$$\langle i|\hat{\boldsymbol{N}} \cdot \hat{\boldsymbol{S}}|f\rangle = \delta_{FF'}\delta_{M_F M_F'}\delta_{LL'}\delta_{NN'}\delta_{JJ'}(-1)^{N+S+J}\left[S(S+1)(2S+1)N(N+1)(2N+1)\right]^{1/2} \begin{Bmatrix} N & S & J \\ S & N & 1 \end{Bmatrix} \tag{7}$$

and

$$\langle i|\left(3\hat{S}_\xi^2 - \hat{\boldsymbol{S}}^2\right)|f\rangle = \delta_{FF'}\delta_{M_F M_F'}\delta_{LL'}\delta_{JJ'}(-1)^{J+S}\left[30(2N+1)(2N'+1)\right]^{1/2} S(S+1)(2S+1)$$
$$\times \begin{pmatrix} N & 2 & N' \\ 0 & 0 & 0 \end{pmatrix} \begin{Bmatrix} S & S & 1 \\ 2 & 1 & S \end{Bmatrix} \begin{Bmatrix} J' & N' & S \\ 2 & S & N \end{Bmatrix}. \tag{8}$$

As in pure O_2, (7) is completely diagonal, but (8) mixes states differing by 2 in N. Both expressions can be simplified by use of the special values for 3-j and 6-j symbols [17], for example

$$\langle i|\hat{\boldsymbol{N}} \cdot \hat{\boldsymbol{S}}|f\rangle = \tfrac{1}{2}\delta_{if}\left[J(J+1) - S(S+1) - N(N+1)\right]. \tag{9}$$

With these matrix elments, a secular matrix for each F and p can be constructed and diagonalised giving the spin coupled ro-vibrational states for those quantum numbers.

No electric dipole transitions are possible in oxygen; however, the magnetic dipole moment of two Bohr magnetons allows magnetic dipole transitions. The perturbative hamiltonian inducing these transitions is the same as the one which causes the first-order Zeeman splitting of the levels in a weak magnetic field [19]

$$\hat{H}' = -g_e \mu_B \hat{S} \cdot \boldsymbol{B}, \tag{10}$$

where μ_B is the Bohr magneton (1.39961 MHz/G) and g_e is 2.00232 [15]. The transition intensity is thus proportional to $|\langle i|\hat{S}|f\rangle|^2$ and a Boltzmann factor which we discuss in section 4. Taking the z axis as the direction of $\boldsymbol{B}$, the relevant matrix element is

$$\langle i|\hat{S}_z|f\rangle = \delta_{M_I M_I'}\delta_{LL'}\delta_{NN'}(-1)^{L+S+N-M_F}[(2F+1)(2F+3)(2J+1)(2J+3)S(S+1)(2S+1)]^{1/2}$$
$$\times \begin{pmatrix} F & 1 & F' \\ -M_F & 0 & M_F' \end{pmatrix} \begin{Bmatrix} J & 1 & J' \\ F' & L & F \end{Bmatrix} \begin{Bmatrix} S & 1 & S \\ J' & N & J \end{Bmatrix}. \tag{11}$$

which contains the selection rules $\Delta F = 0, \pm 1$ and $\Delta M_F = 0$. Eq. (11) is only non-zero for $|F - F'|$ and $|J - J'| \leqslant 1$ and reduces to the familiar form for O_2 [15,19] by substituting $L = 0$.

Again, $\langle i|\hat{S}_z|f\rangle$ can be written as five special cases by using the special values of the 3-j and 6-j symbols. We however will only comment on the M_F dependence of these. When $\Delta F = 0$, the matrix elements are all simply proportional to M_F. This causes the familiar first-order Zeeman levels which are equally spaced; see for example ref. [12]. It also means that $\Delta F = 0$ transitions with $M_F = 0$ (e.g. $F = 0 \leftrightarrow F' = 0$) are forbidden and those with $M_F = F$ are the most intense. For $F \rightarrow F + 1$ transitions, all matrix elements are proportional to $[(F+1) - M_F^2]^{1/2}$ which means that those with $M_F = 0$ are the most intense.

3. Calculated fine-structure spectrum

A test calculation for $F = 0$ and p even showed that a basis set with $N \leqslant 7$ and $q \leqslant 4$ was well saturated. Increasing either N_{max} or q_{max} lowered none of the lowest five levels by more than 0.3 GHz; a test run with $F = 15$ gave the same result.

Calculations were thus performed with this basis for the potentials of Mingelgrin and Gordon (MG) [13] and Pirani and Vecchiocattivi (PV) [14] for F values up to 15. The MG potential was found to be considerably deeper than that of PV, the ground state ($F = 0$, p odd) lying at -3000.24 GHz compared with -2614.16 GHz. We, however, are interested in the fine-structure transitions between low-lying states. Table 1 compares the transition frequencies of all the allowed transitions from the low-lying states with $F \leqslant 2$.

In pure oxygen, the corresponding fine-structure transitions are clustered in the region 56–62 GHz with one transition at 118.75 GHz [11]. Our dimer calculations reproduce these transitions if the anisotropic term, V_2, in the potentials is switched off. The anisotropy in the potential is thus responsible for a drastic change in the fine-structure spectrum upon complex formation. Inspection of the eigenvectors for the complex levels shows the basis functions to be strongly mixed with no nearly good quantum numbers – unlike pure O_2 where N is nearly good or the vector model which assumes J and L to be good [10]. This suggests that an experimental observation of these fine-structure transitions is capable of yielding sensitive information about the anisotropic potential of the van der Waals complex.

Table 1 shows there to be a difference of nearly 400 GHz in the binding energies between the levels in the two potentials considered. Despite this, the calculated fine-structure transitions are in good agreement, with differences often less than 1 GHz. This is more surprising when the anisotropies of the two potentials are compared (see fig. 1, ref. [14]) as the MG potential is markedly more anisotropic than that of PV in the

Table 1
Frequency and relative transition strengths of the allowed ($\Delta F = 0, \pm 1$, parity conserved) fine-structure transitions in O_2Ar for the low-lying states calculated using the potentials of Mingelgrin and Gordon (MG) [13] and Pirani and Vecchiocattivi (PV) [14]. The energies of the lower states relative to the dissociated van der Waals complex are given for comparison

F		Parity	Transition frequency (GHz) [a]		Transition strength PV	Energy (GHz) [a]	
$\|i\rangle$	$\|f\rangle$		PV	MG		PV	MG
2	3	e	11.44	11.89	0.418	−2562.78	−2948.69
2	2	o	39.59	39.34	0.022	−2602.36	−2988.01
1	2	e	47.44	47.47	0.012	−2610.22	−2996.16
2	3	o	50.14	51.12	0.379	−2602.36	−2988.01
2	1	e	52.87	54.46	0.949	−2562.78	−2948.69
2	2	e	58.37	59.80	0.362	−2562.78	−2948.69
2	3	e	74.97	77.41	0.049	−2562.78	−2948.69
2	2	e	76.01	77.29	0.041	−2562.78	−2948.69
2	1	o	91.20	92.32	0.014	−2602.36	−2988.01
1	1	e	100.31	101.94	0.488	−2610.22	−2996.16
2	2	o	101.35	102.98	0.805	−2602.36	−2988.01
0	1	o	103.00	104.55	0.515	−2614.16	−3000.24
2	1	o	105.33	105.78	0.877	−2602.36	−2988.01
1	2	e	105.81	107.27	0.946	−2610.22	−2996.16
1	0	e	107.88	108.22	0.357	−2610.22	−2996.16
2	3	o	108.57	109.99	1.366	−2602.36	−2988.01
0	1	o	117.13	118.01	0.145	−2614.16	−3000.24
1	2	e	123.45	124.76	0.174	−2610.22	−2996.16
2	3	o	130.44	132.19	0.096	−2602.36	−2988.01

[a] 1 cm^{-1} = 29.97925 GHz.

region of the minimum of V_0. In contrast the (comparatively modest) reduction of the PV V_2 by one half perturbs the transitions by $\approx 10\%$.

The transitions shown in table 1 all arise from low-lying vibrational states. The anisotropy of both the PV and MG potential causes these states to be predominantly localised about the perpendicular ($\theta = 90°$) geometry, in agreement with the Henderson and Ewing [20] analysis of their infrared spectrum. The similarity of these spatial distributions partially accounts for the similarity of the spectra.

As the potentials give similar results and that of PV can be regarded as more reliable, being fitted to the results of several experiments, we use this potential for the results presented in the remainder of this work.

Table 1 also gives the relative transition strengths for the transitions calculated using the PV potential. These numbers correspond to $\Sigma_{M_F}|\langle i|\hat{S}_z|j\rangle|^2$ and were thus calculated assuming all M_F levels to be degenerate. In practice, the earth's magnetic field may remove this degeneracy and different strengths for each M_F will be observed. These can be obtained from the values given in table 1 by using the M_F dependence of $\langle i|\hat{S}_z|f\rangle$ given in the previous section.

The relative transition strengths presented in table 1 vary by as much as a hundred between different transitions. This suggests that certain of the transitions listed are considerably more likely to be detectable than others.

Fig. 2 presents smoothed probability distributions as a function of temperatures. These were calculated by including all states with $F \leqslant 15$ which lay below −1500 GHz (77 K). This ensured that the normalising sum over the states was well converged. We note that "high-temperature" O_2Ar spectra such as the one measured by Henderson and Ewing at 93 K sample a large number of ro-vibrational states making their

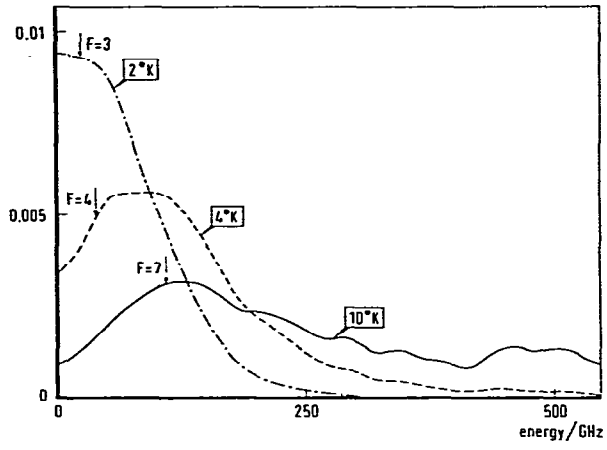

Fig. 2. Probability of finding the O_2Ar complex in a given energy region for several temperatures. The curves are smoothed and are normalised to unity. The state with the largest probability of occupation for each temperature is labeled by its F quantum number.

Table 2
Partition function Z of O_2 and O_2Ar at different temperatures

	Temperature (K)					
	2	4	6	8	10	15
O_2	2.3	4.2	5.6	7.1	8.3	11.9
O_2Ar	40	128	244	385	526	–

quantitative analysis difficult. Also marked in fig. 2 are the states which have the greatest population for each temperature.

Next we estimate the SNR (signal-to-noise ratio) of the dimer spectral lines compared to that of pure oxygen. The square of this relative SNR is proportional to the ratio of the Boltzmann populations, the ratio of the transition strengths and machine-dependent factors such as the number of dimers relative to the number of O_2 monomers. Table 2 shows the partition functions,

$$Z = \sum_{\alpha,F} (2F+1) \exp[-E(\alpha, F)/kT],$$

at several temperatures for O_2 and O_2Ar. Table 2 suggests that the partition function would cause a ten-fold reduction in intensity for an O_2Ar spectrum at 4 K compared to a pure O_2 spectrum at 15 K, realistic experimental temperatures. The transition strengths of the stronger dimer lines (those which do not couple strongly to $J=0$) are similar to those of pure oxygen. For example, the O_2 $N=1$, $J=1\rightarrow 2$ transition has a strength of 0.83 (compare with table 1). The major reduction in relative signal-to-noise ratio will be caused by the smaller number of dimers in, for example, a nozzle expansion, compared with pure O_2, and any lowering of machine sensitivity.

4. Zeeman splittings

We have calculated the splittings of our levels in a weak magnetic field using the perturbative hamiltonian (10). Table 3 presents our results for the lowest states with $F \leqslant 3$. As the selection rule for pure

Table 3
First-order Zeeman splittings, eq. (10), of the low-lying states calculated using the potential of Pirani and Vecchiocattivi. The dissociation energy of the unperturbed state is given for comparison

F	Parity	Energy (GHz)	$\langle \tilde{S}_z \rangle$
1	e	−2610.22	0.0374
1	o	−2511.16	0.2838
2	e	−2562.78	0.3620
2	o	−2602.36	0.3817
3	e	−2590.58	0.0393
3	o	−2551.41	0.2122
15	e	−2152.99	0.0220

Zeeman transitions is $\Delta M_F = \pm 1$, we predict the transition frequencies to be $g_e \mu_B B$ times the splitting (which is a dimensionless quantity).

In pure O_2 the Zeeman splitting decreases with increasing J [12] and analysis of our matrix elements suggests the splittings in the dimer decrease with increase F. To illustrate this, the result with $F = 15$ has been included in table 3. However, two of the low-lying levels, $F = 1$ e and $F = 3$ e, show splittings an order of magnitude smaller than the other low F states. Analysis of the eigenvectors of these states shows that they are dominated by $J = 0$ basis functions, which give zero Zeeman splitting. This means small Zeeman splitting can be observed not only from states with large F but also from states which are predominantly $J = 0$.

5. Conclusions

In this work we have compared the O_2Ar fine-structure spectra calculated using two empirical potentials [13,14]. The predicted spectra are in good agreement despite differences in the potentials, which are reflected in the energy levels. These spectra bear little resemblance to the fine-structure spectrum of pure O_2; they are strongly perturbed by the anisotropy in the interaction potential. Measurements of the O_2Ar spectrum could thus provide valuable information about the anisotropy in the potential and could test whether higher (V_4) terms in the Legendre expansion of the potential are indeed insignificant. A computer programme (see ref. [21]), such as the one used in this paper, which provides a fast and reliable method of generating spectra from a potential can easily be used in the fashion of le Roy and van Kranendonk [2] as a method of inverting experimental data to give information about the potential.

We have also calculated transition intensities, relative signal-to-noise ratios, Boltzmann populations of dimer states at several temperatures and weak-field Zeeman splittings. All these should encourage the observation of both fine-structure and Zeeman spectra of O_2Ar and experimental work on this is now in progress [22].

Acknowledgement

We thank Professor J. Reuss for suggesting the problem, Geert Brocks for making available his programme for generating numerical basis sets and Professor Ad van der Avoird for his careful reading of the manuscript.

References

[1] R.J. le Roy and J. Carley, Advan. Chem. Phys. 42 (1980) 353;
J. Chem. Soc. Faraday Discussions, 73 (1982).
[2] R.J. le Roy and J. van Kranendonk, J. Chem. Phys. 61 (1974) 4750.
[3] A.M. Dunker and R.G. Gordon, J. Chem. Phys. 64 (1976) 354; 68 (1978) 700.
[4] S.L. Holmgren, M. Waldman and W. Klemperer, J. Chem. Phys. 67 (1977) 4414; 69 (1978) 1661.
[5] J. Tennyson and B.T. Sutcliffe, J. Chem. Phys. 77 (1982) 4061.
[6] J. Tennyson and A. van der Avoird, J. Chem. Phys. 77 (1982) 5664.
[7] G.H.L.A. Brocks and J. Tennyson, J. Mol. Spectry., to be published.
[8] J. Verberne and J. Reuss, Chem. Phys. 50 (1980) 137; 54 (1981) 189.
[9] M. Waaijer, M. Jacobs and J. Reuss, Chem. Phys. 63 (1981) 257;
M. Waaijer and J. Reuss, Chem. Phys. 63 (1981) 263.
[10] M. Waaijer, M. Jacobs and J. Reuss, Chem. Phys. 63 (1981) 247.
[11] W.M. Welch and M. Mizushima, Phys. Rev. A5 (1972) 2692.
[12] A. Amirav, U. Even, J. Jortner and L. Kleinman, J. Chem. Phys. 73 (1980) 4217.
[13] V. Mingelgrin and R.G. Gordon, J. Chem. Phys. 70 (1979) 3828.
[14] F. Pirani and F. Vecchiocattivi, Chem. Phys. 59 (1981) 387.
[15] M. Mizushima, The theory of rotating diatomic molecules (Wiley, New York, 1975) ch. 5.
[16] A. Messiah, Quantum mechanics, Vol. 2 (North-Holland, Amsterdam, 1961) p. 1076–1078.
[17] A.R. Edmonds, Angular momentum in quantum mechanics, 2nd Ed. (Princeton, Univ. Press, Princeton, 1960).
[18] I.C. Percival and M.J. Seaton, Proc. Cambridge Phil. Soc. 53 (1957) 654.
[19] M. Tinkham and M.W.P. Strandberg, Phys. Rev. 97 (1955) 937, 951.
[20] G. Henderson and G. Ewing, J. Chem. Phys. 59 (1973) 2280.
[21] J. Tennyson, Computer Phys. Commun., to be published.
[22] J. Mettes, D. Lainée and J. Reuss, private communication.